

https://doi.org/10.1070/QEL16612

Long-range 3D imaging of highly dynamic objects using the intensity ratios of partial beams of reflected laser light

V.I. Ivanov, N.I. Ivanov

Abstract. **The procedural aspects of obtaining long-range three-dimensional images of highly dynamic objects using the ratios of partial beam intensities of the reflected laser light are considered. Alongside with the object images, the proposed method simultaneously provides the data on the object relief with high resolution on a set of surface points during a single-pulse location cycle. The high resolving power and speed of the method ensure the efficiency of its application to detecting and recognition of remote highly dynamic objects, including low-dimensional ones, by their 3D characteristics.**

Keywords: *3D lidar, 3D images, 3D cameras.*

1. Introduction

The appearance of a new generation of compact pulsed lasers and high-sensitivity multielement photodetectors, as well as the growing demand for special kinds of novel instrumentation stimulated the activity in the field of laser location systems aimed at efficient detection, tracking, and recognition of highly dynamic objects in various media [1–6]. For most systems, the functioning algorithms are based on long-range three-dimensional imaging of objects. The solution of this problem is essentially complicated for highly dynamic objects that require development and upgrade of high-speed methods of long-range 3D imaging and image processing. In the present paper, we study a modified algorithm of the laser 3D location method using the ratios of intensities of the partial laser beams in the two-dimensional intensity distribution of the reflected field. We estimate the potentialities of the method in application to long-range 3D imaging of highly dynamic objects. The basic concept of the method was first proposed in Refs [7, 8], and the method itself was used for the first time in Refs [9–11].

2. Theory

To simplify further considerations, we assume that the surface of the located object situated at a distance R_{01} from the lidar is irradiated with the diverging laser light consisting of rectangular pulses. The duration of the probe pulses should satisfy the condition

$$\tau_p > 2\xi_{max}(\boldsymbol{r}_1)/c, \quad (1)$$

where $\xi_{max}(\boldsymbol{r}_1)$ is the maximal elevation of the object surface relief; and c is the velocity of light.

The 3D location method geometry is schematically presented in Fig. 1. The coordinates in the image plane of the optical system (OS) of the lidar are introduced in such a way that the coordinates x, y of the point at the located surface and the coordinates x, y of its paraxial image are related by the simple expression

$$\boldsymbol{S} = \beta \boldsymbol{r}_1, \quad (2)$$

where $\beta = d/R_{01}$ is the magnification factor of the lidar receiving OS; d is the distance from the OS lens to the image plane, where the 2D CCD image detector is placed; $\boldsymbol{S}$ is the radius vector in the image plane of the lidar; and $\boldsymbol{r}_1$ is the radius vector in the object plane.

Since the duration of the laser pulses is small, the state of the located object on the sensing path can be considered 'frozen'. For a diffusely reflecting surface of the object, the light field amplitude in the image plane of the receiving optics is

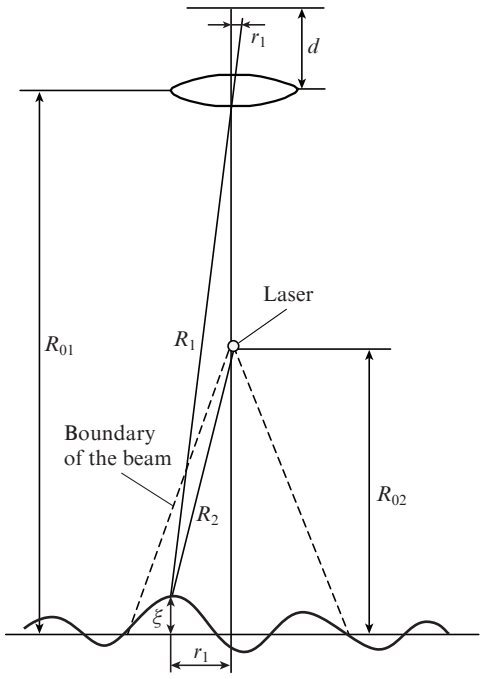

Figure 1. Schematic of the 3D location method geometry.

V.I. Ivanov, N.I. Ivanov Institute for Nuclear Problems, Belarusian State University, ul. Bobruiskaya 11, 220030 Minsk, Belarus; e-mail: ivanov.inp@gmail.com

Received 16 January 2018; revision received 15 February 2018
Kvantovaya Elektronika **48** (7) 679–682 (2018)
Translated by V.L. Derbov

determined as a sum of the field amplitudes reflected from individual points of the surface in the OS direction:

$$E(\boldsymbol{S}) = \sum_k E_k(\boldsymbol{S}), \tag{3}$$

where $E_k(\boldsymbol{S})$ is the field amplitude in the image of the kth point of the surface. The summation is performed over all k irradiated points of the surface belonging to the visual field of the system. The intensity (illuminance) in the image plane of the receiving optics is determined by the square modulus of expression (3):

$$I(\boldsymbol{S}) = \left|\sum_k E_k^2(\boldsymbol{S})\right| = \sum_k \left|E_k(\boldsymbol{S})\right|^2 + \sum_{k\neq i} E_k^*(\boldsymbol{S}) E_i(\boldsymbol{S}). \tag{4}$$

The first sum in Eqn (4) is a sum of intensities of the laser pulses reflected from individual points of the surface, whereas the second sum describes the interference of the fields of these pulses in the image. To describe the spatiotemporal structure of the radiated and reflected light fields, let us introduce the function $f(t) > 0$ that differs from zero in the time interval, equal to the laser light pulse duration τ_p, and has a maximal value equal to unity. Therefore, the amplitude of the laser light field incident on the located surface can be presented as

$$E_0(\boldsymbol{r}_1, t) = f(t-\tau)E_0(\boldsymbol{r}_1), \tag{5}$$

where $E_0(\boldsymbol{r}_1)$ is the distribution of the complex amplitude of the laser light field at the surface; and τ is the propagation time of the laser pulse from the surface point having the coordinate $\boldsymbol{r}_1$. Now, in analogy with Eqn (4), the spatiotemporal structure of the light field in the image plane of the receiving optics will be determined as follows:

$$I(\boldsymbol{S}, t) = \sum_k f^2(t-\tau_k)\,|E_k(\boldsymbol{S})|^2 + \sum_{k\neq i} f(t-\tau_k) f(t-\tau_i)\, E_k^*(\boldsymbol{S}) E_i(\boldsymbol{S}), \tag{6}$$

where $\tau_k = (R_1 + R_2)/c$ is the time of passing the location path by the laser pulse with reflection from the kth point of the surface (Fig. 1).

In the case of a small visual angle of the lidar receiving optics ($r_1/R_{01} \ll 1$), the quantities R_1 and R_2 with sufficient degree of accuracy can be presented as

$$R_1 \approx R_{01} - \xi(\boldsymbol{r}_1) + r_1^2/(2R_{01}), \quad R_2 \approx R_{02} - \xi(\boldsymbol{r}_1) + r_1^2/(2R_{02}). \tag{7}$$

For the combined lidar optical scheme the emission of laser pulses and the reception of the reflected signals are executed practically at the same point separated by the distance R_0 from the located surface. In this case $R_1 \approx R_2$, and $R_{01} \approx R_{02} = R_0$. With these relations and Eqn (7) taken into account, the arrival time τ_k of the signal reflected from the elevation $\xi_k(\boldsymbol{r}_1)$ of the surface at a certain point k is given by the expression

$$\tau_k = \tau_0 - 2\xi_k(\boldsymbol{r}_1)/c + r_1^2/(cR_0), \tag{8}$$

where $\tau_0 = (R_{01} + R_{02})/c = 2R_0/c$ is the arrival time of the reflected signal, corresponding to the level of the located surface ($\xi = 0$), unperturbed by the surface roughness.

For the parameter $\tau_k' = \tau_0 - \tau_k$, from expression (8) under the condition $r_1^2/(\xi R_0) \ll 1$ it follows that $\tau_k' = 2\tau_0(\boldsymbol{r}_1)/c$. The reflected signal $E_k(\boldsymbol{r}_1, t)$ in the image plane of the lidar is formed by a set of k elementary waves, reflected from k points of the surface in the form $E_k(\boldsymbol{S}, t)$. In this case, the parameter τ_k' characterises the temporal shift of the arrival of each of k elementary reflected waves $E_k(\boldsymbol{r}_1, t)$ of the laser light with respect to the time moment τ_0 and is related to the elevation of the surface relief ξ_k at point k. The distribution of shifts of the arrival times of elementary waves at the multielement photodetector, placed in the image plane of the optical system, has the form

$$\tau_k'(\boldsymbol{S}, t) = 2\xi_k(\boldsymbol{r}_1)/c. \tag{9}$$

The maximal value of the temporal shift $\tau_{k\max}'(\boldsymbol{S}, t)$ is defined in the following way:

$$\tau_{k\max}'(\boldsymbol{S}, t) = 2\xi_{k\max}(\boldsymbol{r}_1)/c. \tag{10}$$

The time t_1 of the arrival of the reflected light field at the photodetector is determined by the arrival time of the signal reflected from the surface point having the maximal relief elevation $\xi_{k\max}(\boldsymbol{r}_1)$. According to relations (8) and (10), we obtain the expression for t_1:

$$t_1 = \tau_0 - \tau_{k\max}'(\boldsymbol{S}, t) = 2R_0/c - 2\xi_{k\max}(\boldsymbol{r}_1)/c = \tau_{k\min}, \tag{11}$$

where $\tau_{k\min} = t_1 - t_0$ is the time interval between the moment of signal arrival t_1 and the moment of sending the laser pulse t_0 (in the present case one can assume $t_0 = 0$).

The reflected light field, projected onto the 2D photodetector of the lidar, consisting of $N = N_x N_y$ elements, can be presented as a set of fields of N partial beams. A partial beam is understood as the reflected laser light, hitting a single element (pixel) of the 2D photodetector of the OS. Each of the partial beams is characterised by its intensity and temporal shift $\tau_k'(\boldsymbol{S}, t)$ in correspondence with Eqn (9), and their number N determines the required spatial resolution in the object plane.

Consider the 2D spatial distribution of intensity (image) $B_1(\boldsymbol{S})$. The distribution $B_1(\boldsymbol{S})$ is obtained by accumulating the intensity during the time, smaller than the duration of realisation T of the reflected light field $E(\boldsymbol{S}, t)$, including the leading or trailing edge of the field pulse. In particular, for the segment of $E(\boldsymbol{S}, t)$ realisation including the leading edge of the field, the distribution $B_1(\boldsymbol{S})$ is found by accumulating the intensity of the reflected light field of each partial beam within the spatiotemporal gate τ_{s1}, for which the duration and temporal position are given by the expression

$$\tau_{s1} \geqslant t_2 - t_1 = \tau_{k\max}' + \Delta\tau, \tag{12}$$

where $t_2 = t_1 + \tau_{k\max}' + \Delta\tau$; and $\Delta\tau$ is the time interval that determines the introduced uncertainty of the cut-off zone of the required realisation segment of the field $E(\boldsymbol{S}, t)$ due to fluctuations of the duration and temporal position of the gating pulse τ_{s1} in the hardware implementation.

For a high-resolving OS, when the interference sum in Eqn (6) can be neglected, the distribution of intensity of the reflected light field $B_1(\boldsymbol{S})$ has the form

$$B_1(\boldsymbol{S}) = K(\boldsymbol{r}_1, t)\, T_a(\boldsymbol{S}, t) A(\boldsymbol{S})\, |E_k(\boldsymbol{S})|^2 \int_{t_1}^{t_2} f^2(t_2 - \tau_k')\,\mathrm{d}t = K(\boldsymbol{r}_1, t)\, T_a(\boldsymbol{S}, t) A(\boldsymbol{S})\, |E_k(\boldsymbol{S})|^2 (t_2 - \tau_k'), \tag{13}$$

where $K(\boldsymbol{r}_1, t)$ is the distribution function of the reflection coefficient of the surface; $T_a(\boldsymbol{S}, t)$ is the transfer function of the laser radiation propagation medium along the location path (atmosphere, hydrosphere); and $A(\boldsymbol{S})$ is the instrument transfer function of the lidar OS.

The factor $|E_k(\boldsymbol{S})|^2(t_2 - \tau'_k)$ in Eqn (13) carries information about the distribution of surface elevations $\xi_k(\boldsymbol{r}_1)$. However, the functions $K(\boldsymbol{r}_1, t)$ and $T_a(\boldsymbol{S}, t)$, which are in most cases unknown, introduce a great error when computing the absolute values of $\xi_k(\boldsymbol{r}_1)$. To determine $\xi_k(\boldsymbol{r}_1)$ under the conditions of *a priori* uncertainty of the functions $K(\boldsymbol{r}_1, t)$ and $T_a(\boldsymbol{S}, t)$, we obtain the second distribution $B_2(\boldsymbol{S})$ by 2D accumulation of the field $E(\boldsymbol{S}, t)$ during its full realisation $T = \tau_p + \tau'_{k\max}$. In this case, the duration of each partial beam of the reflected light with high accuracy equals the duration of the laser pulse τ_p. In this connection, the distribution $B_2(\boldsymbol{S})$ has the form

$$B_2(\boldsymbol{S}) = K(\boldsymbol{r}_1, t)\, T_a(\boldsymbol{S}, t) A(\boldsymbol{S}) |E_k(\boldsymbol{S})|^2 \int_{t_1}^{t_1+T} f^2(T - \tau'_{k\max})\, \mathrm{d}t$$

$$= K(\boldsymbol{r}_1, t)\, T_a(\boldsymbol{S}, t) A(\boldsymbol{S}) |E_k(\boldsymbol{S})|^2 \tau_p. \qquad (14)$$

One can easily see that the distribution $B_2(\boldsymbol{S})$ is a 2D image of the located object with the selection of the backscattered signal background.

From the ratios of the obtained intensities of the partial beams in the distributions $B_1(\boldsymbol{S})$ and $B_2(\boldsymbol{S})$ we find the distribution of temporal shifts $\tau'_k(\boldsymbol{S})$ for the arrival of each of N partial beams of the reflected light in the form

$$\tau'_k(\boldsymbol{S}) = t_2 - \tau_p B_1(\boldsymbol{S})/B_2(\boldsymbol{S}). \qquad (15)$$

From this, with Eqn (9) taken into account, we obtain the desired distributions over N points of the surface of the located object for the relief elevation

$$\xi_k(\boldsymbol{r}_1) = (c/2)[t_2 - \tau_p B_1(\boldsymbol{S})/B_2(\boldsymbol{S})], \qquad (16)$$

and for the distances $R_\xi(\boldsymbol{r}_1)$ to the elevation points

$$R_\xi(\boldsymbol{r}_1) = R_b + \xi_k(\boldsymbol{r}_1), \qquad (17)$$

where R_b is the base distance, determined from the interval $t_1 - t_0$ as a distance to the point of the surface with maximal elevation in correspondence with Eqn (11), namely, $R_b = c(t_1 - t_0)/2 = c\tau_{k\min}/2$.

The images $B_1(\boldsymbol{S})$ and $B_2(\boldsymbol{S})$ may be recorded using a variety of multielement photodetector channels (PDCs), implementing the function of charge accumulation, namely, the CCDs, including those with internal amplification, the arrays of avalanche photodiodes with charge accumulating elements; the hybrid electron-optical converters (EOCs), i.e., the EOCs combined with the CCD cameras.

To measure the base distance R_b, one can use different known methods of time-of-flight ranging with the threshold detection of the moment t_1 of the reflected signal arrival.

3. Results of calculations and experiments

As follows from Eqns (16) and (17), for high-resolving OS of the lidar, the error of determining the absolute values of $\xi_k(\boldsymbol{r}_1)$ and $R_\xi(\boldsymbol{r}_1)$ depends only on the instrumental error, namely, on the error of the quantities t_2, τ_p, $B_1(\boldsymbol{S})$, and $B_2(\boldsymbol{S})$.

The resolving power ξ_r of determining the relief elevation is the main parameter in the 3D ranging. The equation for evaluating ξ_r is derived by us in the form

$$\xi_r = \xi_{k\max}/D_d + c\Delta\tau/(2D_d), \qquad (18)$$

where D_d is the linear dynamic range of the PDC sensitivity.

As follows from expression (18), the resolving power ξ_r is improved with the growth of D_d and achieves the best value under the minimisation of $\Delta\tau$ [$\Delta\tau \to 0$ in Eqn (12)].

The PDCs based on a CCD and a hybrid EOC of the fifth generation with the electronic excitation of the CCD provide the widest dynamic range of $D_d \geqslant 10^3$, and for the hybrid EOCs with a luminescent screen, $D_d \approx (0.8-1.5) \times 10^2$. The estimate of the resolving power, obtained using Eqn (18) for $D_d = 500$ and the maximal elevation of the surface relief $\xi_{k\max} = 3$ m, which is typical for recognition of most airborne, ground-based, and submarine objects, amounts to ~6 mm.

The experimental determination of the resolving power ξ_r was performed for test objects measuring 80 cm × 80 cm with a stepped calibrated profile of elevations with $\xi_{k\max} = 30$ cm at the distance up to 1 km. The diffuse reflection coefficient of the object was equal to 0.24–0.3; the duration of laser pulses was $\tau_p = 30$ ns; the used PDC was an EOC with a microchannel plate and a luminescent screen, combined with a CCD matrix. The dynamic range of the PDC was $D_d \approx 90$; the discrete dimensions of the analysed area in the object plane were $N = 128 \times 128$ elements. The experimental estimates of root-mean-square error σ_ξ, obtained from 10 measurements in the range of elevations $\xi_k(\boldsymbol{r}_1) = 0-30$ cm at $N \approx 1.6 \times 10^4$ points of the test object surface did not exceed 7 mm. Figure 2 presents histograms of the probability density distribution for the absolute value of error $\pm\Delta\xi$ for 100 measurements.

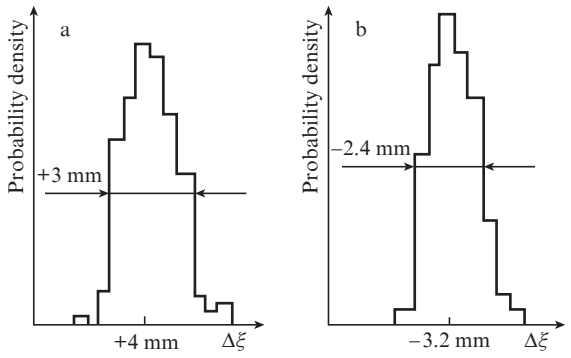

Figure 2. Histograms of the probability density distribution of the absolute value of the error (a) $+\Delta\xi$ and (b) $-\Delta\xi$.

The spatial resolution r_r in the plane of the test object having the area 6400 cm^2 was ~0.4 cm^2. The time of acquiring long-range 3D images was reduced by more than N times, compared to the laser location systems of point-by-point scanning, based on time-of-flight or phase measurements.

The considered method allows the relief elevations $\xi_k(\boldsymbol{r}_1)$ to be determined at a large number N of the object surface points, which can amount to tens and hundreds of thousands

depending on the number of simultaneously detected partial beams of the reflected laser light. The modern matrix detectors for the visible and near-IR ranges comprise millions of pixels, so that the number N, determining the number of the above beams and therefore the speed of operation and the spatial resolution in the object plane, is restricted only by diffraction phenomena and energy potential of the lidar, the requirements to which at the given range of location grow with increasing N.

4. Conclusions

The obtained results confirm the high resolution and operation speed of the method of long-range 3D imaging using the intensity ratios of the partial beams of the reflected laser light. The high accuracy and operation speed, as well as the possibility of implementing the method using the domestically produced element base, offer the prospects of its application for increasing the efficiency of detection and recognition of a wide class of highly dynamic airborne, underwater, and ground-based objects by their 3D characteristics, related to the solution of a number of special-purpose problems [1–6], including the detection of antiamphibious mesh and grid underwater entanglements. The method can also be applied in helicopter-based systems for detecting electric wires, in the systems for automated landing of different aircrafts onto uneven surfaces, in the diagnostics of parameters of small-scale surface waves on the sea surface, and in a number of other problems.

References

1. Katenin V.A. *Ekspertnyi Soyuz*, **6** (30), 25 (2012).
2. Shcherbakov V.V. *Obozreniye Armii i Flota*, **3** (46), 46 (2013).
3. Boreisho A.S. (Ed.) *Voyennoye primeneniye lazerov* (Military Applications of Lasers) (Saint-Petersburg: Baltic State Technical University, 2015) p. 103.
4. Karasik V.E., Orlov V.M. *Lokatsionnye lazernye sistemy videniya* (Location Systems of Laser Vision) (Moscow: Bauman Moscow State Technical University, 2013) p. 478.
5. Wood J.J., Randall P.N., Nicholas M.R., Nothard J.M., Watson G.H., Harvey C., Smith G. *Proc. SET 130. NATO Military Sensing Symposium* (Orlando, USA, 2008) p. 147.
6. Belov V.V., Abramochkin V.N., Gridnev Y.V., Kudryavtsev A.N., Tarasenkov M.V., Fedosov A.V. *Atmos. Ocean. Opt.*, **30** (4), 366 (2017) [*Opt. Atmos. Okeana*, **30** (4), 285 (2017)].
7. Ivanov V.I. Patent SU 1593429 A1, G01S17/00. Priority of 04.01.1988.
8. Ivanov V.I. Patent SU 159 1621 A1, G01C3/08. Priority of 11.04.1988.
9. Ivanov V.I., in *Metody i sredstva distantsionnogo zondirovaniya Zemli i obrabotki kosmicheskoi informatsii v interesakh narodnogo khozyaystva* (Methods and Means of the Earth Remote Sensing and Processing of Space Information in the Interests of National Economy) (Ryazan, 1989) Pt 1, p. 39.
10. Ivanov V.I., in *Problemy kompleksnoy avtomatizatsii gidrofizicheskikh issledovaniy* (Problems of Complex Automation of Hydrophysical Studies) (Sevastopol, 1989) p. 171.
11. Ivanov V.I., in *Vysokoskorostnaya fotografiya, fotonika i metrologiya bystroprotekayushchikh protsessov* (High-Speed Photography, Photonics and Metrology of Fast Processes) (Moscow, 1989) p. 114.